# Informing direct neutron capture on tin isotopes near the N=82 shell closure

B. Manning, G. Arbanas, J. A. Cizewski, R. L. Kozub, S. Ahn, J. M. Allmond, D. W. Bardayan, K. Y. Chae, K. A. Chipps, M. E. Howard, K. L. Jones, J. F. Liang, M. Matos, C. D. Nesaraja, F. M. Nunes, P. D. O'Malley, S. D. Pain, W. A. Peters, S. T. Pittman, A. Ratkiewicz, K. T. Schmitt, D. Shapira, M. S. Smith, and L. Titus

Phys. Rev. C **99**, 041302 — Published 18 April 2019

DOI: 10.1103/PhysRevC.99.041302

# Informing Direct Neutron Capture on Tin Isotopes Near the $N = 82$ Shell Closure

B. Manning,[1,2] G. Arbanas,[3] J.A. Cizewski,[1] R.L. Kozub,[4] S. Ahn,[5,6,7] J.M. Allmond,[8] D.W. Bardayan,[8,9] K.Y. Chae,[10] K.A. Chipps,[11,8] M.E. Howard,[1] K.L. Jones,[5] J.F. Liang,[8] M. Matos,[12] C.D. Nesaraja,[8] F.M. Nunes,[6] P.D. O'Malley,[1,9] S.D. Pain,[8] W.A. Peters,[13] S.T. Pittman,[5,13] A. Ratkiewicz,[1] K.T. Schmitt,[5] D. Shapira,[8] M.S. Smith,[8] and L. Titus[6]

[1] *Department of Physics and Astronomy, Rutgers University, New Brunswick, New Jersey 08903, USA*
[2] *Physics Division, Los Alamos National Laboratory, Los Alamos, NM 87545, USA*
[3] *Reactor and Nuclear Systems Division, Oak Ridge National Laboratory, Oak Ridge, Tennessee 37831-6171, USA*
[4] *Department of Physics, Tennessee Technological University, Cookeville, Tennessee 38505, USA*
[5] *Department of Physics and Astronomy, University of Tennessee, Knoxville, Tennessee 37996, USA*
[6] *Department of Physics and Astronomy, Michigan State University, East Lansing, MI 48824, USA*
[7] *JINA-CEE, Michigan State University, East Lansing, MI 48824, USA*
[8] *Physics Division, Oak Ridge National Laboratory, Oak Ridge, TN 37831, USA*
[9] *Department of Physics, University of Notre Dame, South Bend, IN 46556, USA*
[10] *Department of Physics, Sungkyunkwan University, Suwon 440-746, Korea*
[11] *Department of Physics, Colorado School of Mines, Golden, Colorado 80401, USA*
[12] *Department of Physics and Astronomy, Louisiana State University, Baton Rouge, LA 70803, USA*
[13] *Oak Ridge Associated Universities, Oak Ridge, Tennessee 37831, USA*

(Dated: January 4, 2019)

Half of the elements heavier than iron are believed to be produced through the rapid neutron capture process ($r$-process). The astrophysical environment(s) where the $r$-process occurs remains an open question, even after recent observations of neutron star mergers and the associated kilonova. Features in the abundance pattern of $r$-process ashes may provide critical insight for distinguishing contributions from different possible sites, including neutron star mergers and core-collapse supernovae. In particular, the largely unknown neutron capture reaction rates on neutron-rich unstable nuclei near $^{132}$Sn could have a significant impact on the final $r$-process abundances. To better determine these neutron capture rates, the $(d, p)$ reaction has been measured in inverse kinematics using radioactive ion beams of $^{126}$Sn and $^{128}$Sn and a stable beam of $^{124}$Sn interacting with a $(CD_2)_n$ target. An array of position-sensitive silicon strip detectors, including the Super Oak Ridge Rutgers University Barrel Array, was used to detect light reaction products. In addition to the present measurements, previous measurements of $^{130,132}$Sn$(d, p)$ were reanalyzed using state-of-the-art reaction theory to extract a consistent set of spectroscopic factors for $(d, p)$ reactions on even tin nuclei between the heaviest stable isotope, $^{124}$Sn, and doubly magic $^{132}$Sn. The spectroscopic information was used to calculate direct-semidirect $(n, \gamma)$ cross sections, which will serve as important input for $r$-process abundance calculations.

PACS numbers: 21.10.Jx, 25.45.Hi, 25.60.Je, 26.30.Hj

Synthesis in the cosmos of elements heavier than iron is still not fully understood [1–4]. Nearly half of these heavy elements are synthesized via the rapid neutron-capture process ($r$-process) [5]. The recent observation of the gravitational waves from a binary neutron-star merger [6] and the subsequent kilonova understood to be powered by the decay of rare-earth elements [7, 8] demonstrates that binary neutron-star mergers are an important $r$-process site. However, the $r$-process path varies, depending on the astrophysical conditions, resulting in different abundance patterns [9–11].

In a "cold" $r$-process, which could occur in neutron-star mergers or a highly accelerated neutrino-driven wind, equilibrium between neutron capture and photodissociation rapidly breaks down, long before the neutrons from the neutron-rich environment are exhausted. The timescales of the cold $r$-process are such that the competition between neutron capture and beta decay occurs during the bulk of the $r$-process nucleosynthesis. Under these conditions neutron-capture rates along the $r$-process path play a critical role in the final abundance pattern [11–15]. The traditional, or "hot", $r$-process path is thought to take place in the neutrino-driven winds from a proto-neutron star resulting from a core-collapse supernova. This $r$-process path begins in $(n, \gamma)$-$(\gamma, n)$ equilibrium [16, and references therein] and remains there for considerable time, such that neutron separation energies play an important role in the nucleosynthesis [17]. However, during freeze-out from a hot $r$-process, equilibrium between neutron capture and photodissociation again breaks down and the final abundance pattern predictions are sensitive to unknown $(n, \gamma)$ cross sections on hundreds of unstable nuclei [11–15].

An important difference between the various hot and cold r-process abundance patterns is the $A \sim 130$ peak. In the hot $r$-process, this peak is narrow and centered above $A = 130$; in the cold $r$-process, in contrast, the peak is much broader and centered lower in mass [15]. In

particular, in cold neutrino-driven winds and in neutron star mergers, the sensitivity of the final abundances to unknown $(n,\gamma)$ rates in tin isotopes below the $N = 82$ shell closure is substantially increased over hot $r$-process sites [11], in some cases by as much as a factor of 10. Cold $r$-process abundances are also sensitive to a larger number of neutron capture rates than the hot r-process [11], making systematic studies across isotopic chains a key piece of understanding $r$-process nucleosynthesis.

The advent of radioactive ion beams (RIBs) has enabled studies of nuclei far from stability. Transfer reactions on isotopes near doubly magic $^{132}$Sn, with $Z = 50$ and $N = 82$ [18–21], have been of particular interest as they probe the nuclear shell model away from stability. The relatively long $\beta$-decay half-lives of $A \approx 130$ neutron-rich isotopes near the $r$-process path increases the importance of their $(n,\gamma)$ rates in calculating $r$-process nucleosynthesis at late times [12, 13]. For nuclei where $(n,\gamma)$ cannot be directly measured, the rates are often calculated using a Hauser-Feshbach (HF) model. However, HF calculations can have large uncertainties and are not applicable when the nuclear level density and/or neutron separation energy are low. For nuclei with low level densities, such as near shell closures or when the neutron separation energy is low, neutron capture is expected to be dominated by direct capture into single-neutron states via the direct-semidirect (DSD) mechanism [22–25]. Empirical spectroscopic factors, S, for final neutron bound states are needed to calculate DSD $(n,\gamma)$ cross sections for nuclei near the $r$-process path and informing synthesis of heavy nuclei and the observed abundances. Direct capture is expected to dominate in nuclei with low level densities, such as tin isotopes with $N \geq 82$. For $s$-wave direct neutron capture near $N = 82$, the single-particle properties of the $3p_{3/2}$ and $3p_{1/2}$ states are most important, as they will be preferentially populated via $E1$ transitions. However, these direct capture cross sections can not be directly deduced for nuclei away from stability, and theoretical calculations can vary by as much as three orders of magnitude depending on the chosen model [26]. Spectroscopic factors can also constrain nuclear structure models used to predict properties of nuclei that are not accessible to measurements. Because there are limited capabilities to deduce DSD rates from measured values of S, especially in the more neutron-rich nuclei where they are likely to be dominant, it is important to benchmark the calculations against experiment.

The present study combines previous $(d,p)$ studies on $^{132}$Sn and $^{130}$Sn, with new measurements of the $(d,p)$ reaction on $^{128}$Sn, $^{126}$Sn, and $^{124}$Sn using similar detectors and the same analysis procedures. The $3/2^-$ and $1/2^-$ states at similar $Q$-values in $^{133}$Sn and $^{131}$Sn have been shown to be essentially pure single-neutron $3p_{3/2}$ and $3p_{1/2}$ configurations, respectively [18–21]. This is in contrast to $^{125}$Sn [27] where these same configurations studied using a stable target of $^{124}$Sn in normal kinematics, have been observed to be highly fragmented.

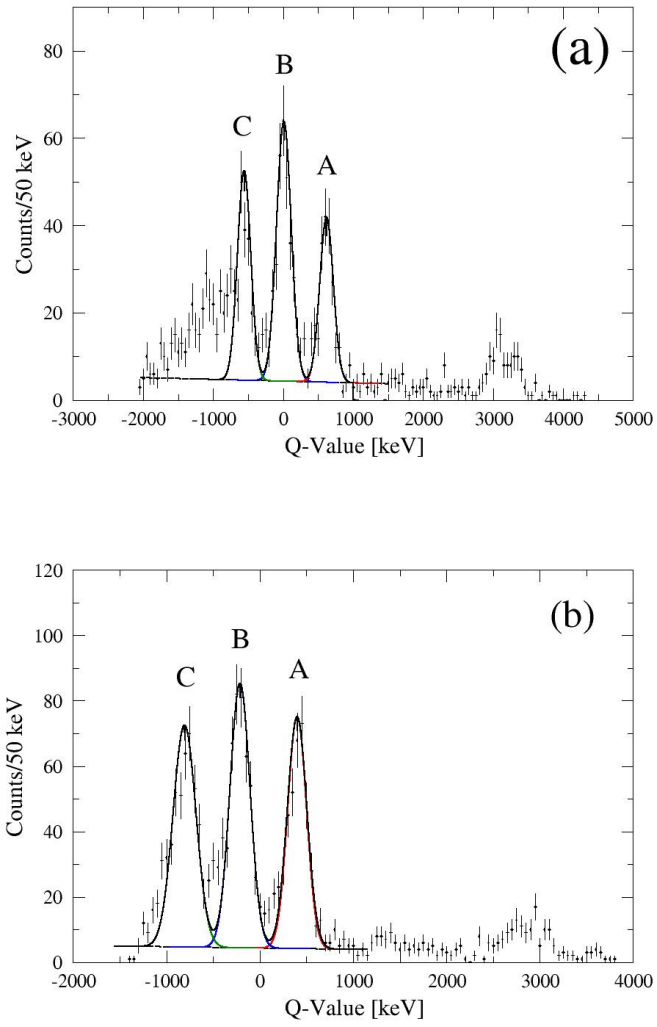


FIG. 1. (color online) $Q$-value spectra of (a) $^{126}$Sn$(d,p)$ and (b) $^{128}$Sn$(d,p)$ reaction measurements in inverse kinematics, summed over all angles. The uncertainties on the data are purely statistical. Colored curves represent the fits to each state and the background. A solid black line represents the sum of all of the fits and the background. The centroids extracted from the individual fits for panel (a) are $Q_A = 0.62 \pm 0.04$ MeV, $Q_B = 0.01 \pm 0.05$ MeV, and $Q_C = -0.56 \pm 0.05$ MeV and for panel (b) are $Q_A = 0.40 \pm 0.05$ MeV, $Q_B = -0.21 \pm 0.05$ MeV, and $Q_C = -0.81 \pm 0.06$ MeV. The uncertainties on the centroids are determined from the error in the fit.

To probe single-neutron excitations in neutron-rich tin isotopes, a stable ion beam of $^{124}$Sn and RIBs of $^{126}$Sn and $^{128}$Sn were produced separately and accelerated to 630 MeV (5.1 MeV/u, 5 MeV/u, and 4.9 MeV/u, respectively), at the Holifield Radioactive Ion Beam Facility at Oak Ridge National Laboratory (ORNL). Thin deuter-

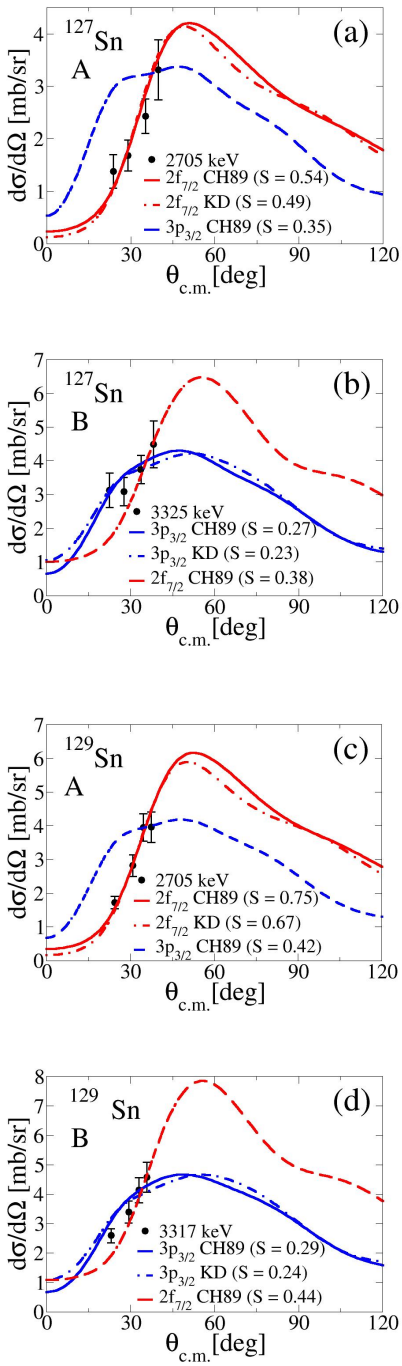


FIG. 2. Typical pairs of $\ell = 3$ and $\ell = 1$ absolute differential cross sections from the $^{126}$Sn$(d,p)$ (panels (a) and (b)) and $^{128}$Sn$(d,p)$ (panels (c) and (d)) reactions with purely statistical uncertainties. Panels (a) and (c) are for states $A$ in Fig. 1 in $^{127}$Sn and $^{129}$Sn, respectively; panels (b) and (d) are for states $B$ in Fig. 1 in $^{127}$Sn and $^{129}$Sn, respectively. The data are compared to FR-ADWA calculations for an angular momentum transfer of $\ell = 3$ (red curves) and $\ell = 1$ (blue curves). Adopted orbital angular momentum transfer calculations were made using the Chapel-Hill parameterization (solid curve) and the Koning-Delaroche (KD) parameterization (dot-dashed curves). The alternate orbital angular momentum transfers ($\ell = 1$ in (a) and (c) and $\ell = 3$ in (b) and (d)) were calculated with the Chapel-Hill 89 parameterization (dashed line). In panel (d), the best fit for state $B$ was for only $\ell = 1$ transfer. A state at 3394 keV with a (1/2,3/2) assignment was previously observed in beta decay. [28]

TABLE I. Spectroscopic information for the $f$- and $p$-wave single-neutron states populated by the $(d,p)$ reaction on neutron-rich tin isotopes. For completeness, the reanalysis of the candidates for the $2f_{5/2}$ states in $^{131}$Sn and $^{133}$Sn is included. The S were extracted using a FR-ADWA formalism and Koning-Delaroche optical model parameters. Only statistical experimental uncertainties in parenthesis are presented. The uncertainties on the excitation energies for $^{131}$Sn and $^{133}$Sn were adopted from work by Kozub *et al.* [20] and Jones *et al.* [19], respectively.

| $^{A}X$ | $E_x$ (keV) | $Q$ (MeV) | $J^\pi$ | S |
|---|---|---|---|---|
| $^{125}$Sn[1] | 2770 (40) | 0.74 | $7/2^-$ | 0.36 (0.03) |
| | 3390 (50) | 0.13 | $3/2^-$ | 0.24 (0.02) |
| | 4000 (50) | -0.49 | $1/2^-$ | 0.34 (0.04) |
| $^{127}$Sn | 2710 (40) | 0.62 | $(7/2)^-$ | 0.49 (0.07) |
| | 3330 (50) | 0.01 | $(3/2)^-$ | 0.23 (0.03) |
| | 3880 (50) | -0.56 | $(1/2)^-$ | 0.43 (0.04) |
| $^{129}$Sn | 2710 (50) | 0.40 | $(7/2)^-$ | 0.67 (0.09) |
| | 3320 (50) | -0.21 | $(3/2)^-$ | 0.24 +0.03/-0.11[2] |
| | 3910 (60) | -0.81 | $(1/2)^-$ | 0.44 (0.07) |
| $^{131}$Sn | 2628 (50) | 0.39 | $(7/2)^-$ | 0.85 (0.11) |
| | 3404 (50) | -0.38 | $(3/2)^-$ | 0.50 (0.11) |
| | 3986 (50) | -0.96 | $(1/2)^-$ | 0.88 (0.14) |
| | 4655 (50) | -1.63 | $(5/2)^-$ | 0.66 (0.12) |
| $^{133}$Sn | 0 | 0.25 | $7/2^-$ | 0.90 (0.07) |
| | 854[3] | -0.61 | $3/2^-$ | 0.87 (0.07) |
| | 1363 (31)[3] | -1.12 | $1/2^-$ | 1.3 (0.3) |
| | 2005[3] | -1.76 | $5/2^-$ | 1.1 (0.3) |

[1] Ref. [27] observed $7/2^-$ states at 2755 and 2798 keV (total S= 0.33), three $3/2^-$ states (total S= 0.25), and four $1/2^-$ states in the range 4009 − 4027 keV (total = 0.30). These values agree well with our values of 0.36(3), 0.24(2), and 0.34(4), respectively.

[2] While the best fit for state $B$ is $\ell = 1$ transfer, there could be up to a 30% $\ell = 3$ component in $^{129}$Sn near $E_x = 3320$ keV, reflected in the quoted uncertainties.

[3] More definitive energies and spins for these states in $^{133}$Sn were recently established with ($^{9}$Be, $^{8}$Be) transfer reaction [21], which also reported $S = 0.9(2)$ for all of these states, consistent with the present results.

ated polyethylene ($CD_2$) foils were deployed: 242 $\mu$g/cm$^2$ for $^{126,128}$Sn beams and 139 $\mu$g/cm$^2$ for $^{124}$Sn. The resolution for the states in $^{127,129}$Sn was degraded ($\approx$ 100 keV) compared to $^{125}$Sn ($\approx$ 80 keV) because of increased beam and proton energy straggling. The foils were held in a thin target ladder, perpendicular to the beam axis, to reduce shadowing of reaction products near 90° in the laboratory. The beam intensity was measured in a newly commissioned $CF_4$-filled tilted-grid ionization chamber (IC) [29] downstream of the targets. The average measured beam intensities were 250,000 pps of $^{124}$Sn, 100,000 pps of $^{126}$Sn, and 35,000 pps of $^{128}$Sn.

The Super Oak Ridge Rutgers University Barrel Array (SuperORRUBA) [30], deployed to detect charged

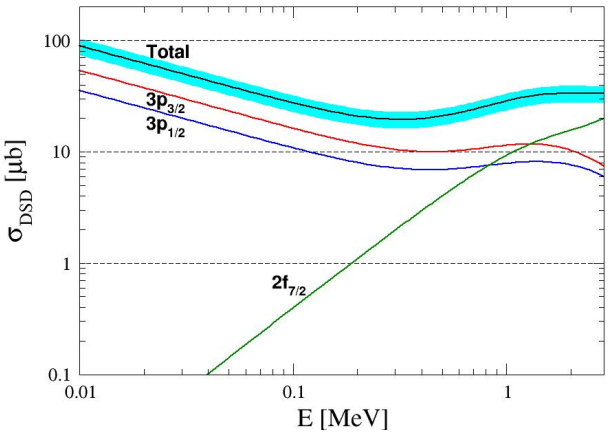


FIG. 3. (color online) Calculation of direct-semidirect neutron capture on $^{128}$Sn. Similar results for capture on $^{124,126,130,132}$Sn were obtained and agree with the previous study of $^{130}$Sn [20]. The teal band represents the uncertainty in the cross section due to the uncertainties in S. $s$-wave direct capture to $\ell = 1$ states dominates the capture at low neutron energies.

particles, consisted of ten 1000 $\mu$m thick silicon detectors covering 55°-89° in the laboratory, and two covering 92°-125°. The experimental setup is described in detail in [31, 32]. In addition to monitoring the beam intensity, the IC was used to identify coincidences between heavy ion recoils and light charged-particles detected in SuperORRUBA, significantly reducing the background in the energy-versus-angle spectra. Proton kinematic curves were converted to $Q$-value spectra in the center of mass. $Q$-value centroids were determined by fitting a Gaussian curve with a nearly flat background to each peak. The results are summarized in Table I and compared to previous results [27] for $^{125}$Sn. The groups listed may contain more than one state, but the angular distributions nonetheless seem to be dominated by a single value of transferred angular momentum, $\ell$.

Figure 1 displays the $Q$-value spectra from the $^{126,128}$Sn$(d,p)$ measurements. The states and their relative spacing are strongly reminiscent of $^{132}$Sn [18, 19] and $^{130}$Sn$(d,p)$ [20] studies with similar $Q$-values. The total beam flux and target thickness were calculated by normalizing the elastically scattered deuterons to elastic scattering calculations for the most forward center of mass angles [19]. Proton data for each $Q$-value group were divided into angular bins and normalized to the total beam flux to extract absolute differential cross sections for each state. Figure 2 displays angular distributions for $^{127,129}$Sn peaks, labeled $A$ and $B$ in Fig. 1.

All of the $(d,p)$ reaction data on even mass tin isotopes from $A = 124 - 132$ were analyzed using the same reaction theory and optical models to extract a consistent set of spectroscopic factors that can be directly compared. The reaction calculations used the code FRESCO [33], employing Finite Range ADiabatic Wave Approximation (FR-ADWA) formalism. A Reid interaction [34] was used for the neutron-potential. The Koning-Delaroche (KD) potential [35] was used for the proton-target and neutron-target systems. Calculations were repeated using the Chapel Hill global potential (CH89) [36] for comparison. The adiabatic potential of the deuteron was calculated using the code TWOFNR [37]. A major source of uncertainty in modeling transfer reactions is the choice of the Woods-Saxon potential parameters for the bound state. Density Functional Theory (DFT) can be used to predict these parameters; however, for the tin isotopes the uncertainties would still be large [38]. Therefore, we employed a Woods-Saxon shaped potential with the same radius parameter $r_0 = 1.25$ fm and diffuseness parameter $a = 0.65$ fm adopted in previous studies [19, 20, 39, 40]. A standard Woods-Saxon spin-orbit potential of 6 MeV was added. The reaction calculations assumed final states of pure single-particle character to determine the spectroscopic factor for each state. Normalizing the calculated differential cross section to the experimental data yields the spectroscopic factor for the given state as shown in Fig. 2 for $\ell = 1$ and $\ell = 3$ transfers to $^{127,129}$Sn. Here, $S = 1$ means that the state is of pure single-particle nature. Tentative $J^\pi$ assignments are supported by the similar $Q$-values and separation of energy levels for the observed states among all 5 tin isotopes and the shapes of the angular distributions. The results of the spectroscopic factor analysis are summarized in Table I.

The DSD calculations were performed with the code CUPIDO [24, 42]. Both real and imaginary parts of the incident channel were calculated using the Koning-Delaroche potential [35]. The neutron bound-state wave function was calculated by varying the depth of a Woods-Saxon potential to reproduce the measured binding energy for each bound state; the geometry was fixed with $r_0 = 1.25$ fm and $a = 0.65$ fm, as was done in the transfer calculations, ensuring consistency.

The excitation energies, spins, parities, and spectroscopic factors used in our DSD calculations are taken from the measurements and summarized in Table I; the Giant Dipole Resonance (GDR) information was taken from recent data evaluations [43]. At low neutron energies, low-spin states will dominate direct neutron capture, as seen in Fig. 3.

Figure 4 displays the present DSD neutron capture cross sections at 30 keV compared with previous theoretical calculations [44] that were made using theoretical excitation energies and unit spectroscopic factors. The present calculations were made using empirical excitation energies and spectroscopic factors. The calculation for neutron capture on $^{132}$Sn at 30 keV agrees with previous calculations [26] within experimental uncertainties. The results for neutron capture on $^{130}$Sn at 30 keV is slightly reduced from that of previous calculations [20]. The discrepancies, due to differences in reaction models, agree

within reported uncertainties. The Ref. [27] experimental energies and spectroscopic factors (deduced with non-global optical model parameters and a different choice of radius and diffuseness parameters) were used to deduce DSD cross sections for $^{124}$Sn. These values are somewhat larger than the present work because states only observed in [27] were included (see Fig. 4 for the value at 30 keV). The difference between the Ref. [44] calculations and the present results was previously noted by Kozub et al. [20], who suggested the differences between current $^{130}$Sn DSD calculations and those in [44] are likely due to using different single-particle level energies and/or the different single-particle bound-state potential by Koura et al. [45]. The HF calculations in Fig. 4 assume a high level density near the neutron separation energy. An open question is the role that Hauser-Feshbach statistical neutron capture plays in the tin isotopes for $N < 82$. While the level density has been measured to be high in $^{125}$Sn (e.g., [2]) and the level density in $^{133}$Sn is low, it is not known when the level density in $124 < A < 132$ Sn nuclei would be sufficiently high for HF statistical capture to dominate over DSD. The experimental techniques to measure (d,p$\gamma$) reactions with radioactive ion beams have been realized [46]. This reaction has been validated [47] as a surrogate for neutron capture. Therefore, the statistical component of (n,$\gamma$) reactions on short-lived nuclei near the $r$-process path can be deduced when accelerated radioactive ion beams of sufficient intensity are available.

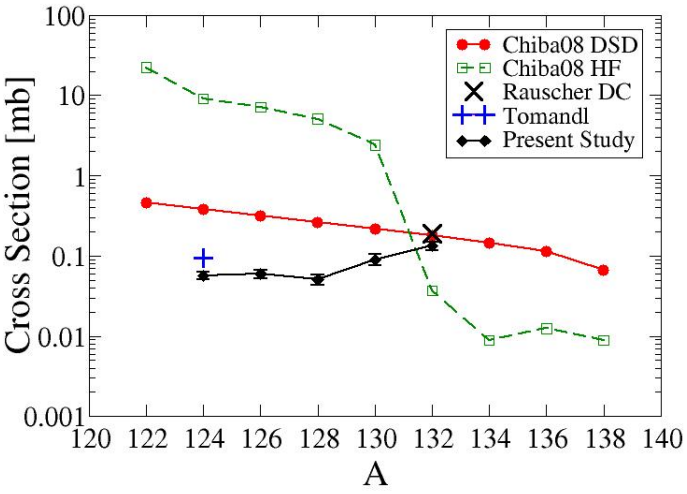


FIG. 4. (color online) Comparison of calculated neutron-capture cross sections for tin isotopes at 30 keV. Present DSD calculations with experimental energies and spectroscopic factors (black diamonds), Hauser-Feshbach model calculations [44] (green squares), $^{132}$Sn direct capture using theoretical spectroscopic factor [26] (black "X"), $^{124}$Sn DSD calculations using spectroscopic factors of [27] for all $\ell = 1$ levels having S $> 0.01$ (blue "+"), and DSD calculations with theoretical excitation energies and spectroscopic factors (red circles) [44].

In summary, radioactive ion beams of $^{126}$Sn and $^{128}$Sn were used to measure the $^{126}$Sn$(d,p)$ and $^{128}$Sn$(d,p)$ reactions for the first time. These were combined with a new measurement of $^{124}$Sn$(d,p)$ and with a re-analysis of previous $^{130,132}$Sn$(d,p)$ studies. Excitation energies and proton differential cross sections were measured for single-neutron states in $^{125}$Sn, $^{127}$Sn, and $^{129}$Sn. Orbital angular momentum transfers and spectroscopic factors were deduced using the same reaction models for the states in $^{125}$Sn, $^{127}$Sn, and $^{129}$Sn, as well as the analogous single-neutron states in $^{131}$Sn and $^{133}$Sn measured previously [18–20]. These spectroscopy results reinforce the need for shell model predictions of excitations in neutron-rich tin isotopes that reproduce empirical results, especially for $3p_{1/2}$ strength. The empirical spectroscopic properties were used to calculate direct-semidirect (DSD) neutron capture cross sections on $^{132}$Sn, $^{130}$Sn, $^{128}$Sn, $^{126}$Sn, and $^{124}$Sn; these results were compared with previous predictions of these cross sections made before the new empirical spectroscopy was available. The present work constrains the previously unknown direct component of neutron capture in neutron-rich tin nuclei near the $r$-process path of nucleosynthesis and highlights the need to determine experimentally the statistical component with a surrogate reaction.

## ACKNOWLEDGEMENTS

This work was supported in part by the U.S. Department of Energy under Contracts No. DE-FG52-08NA28552 and DE-NA0002132 (Rutgers), No. DE-FG02-96ER40983 (UTK), No. DE-SC0001174 (UTK), No. DE-FG02-96ER40955 (TTU), No. DE-AC05-00OR22725 (ORNL), the National Science Foundation under Contract No. NSF-PHY-1067906 and NSF-PHY-1404218 (Rutgers) and NSF-PHY-0555893 (MSU), reactiontheory.org, the TORUS: Theory of Reactions for Unstable iSotopes a DOE Office of Science Topical Collaboration for Nuclear Theory, and the National Research Foundation of Korea (NRF-2016K1A3A7A09005579 and NRF-2016R1A5A1013277). This research used resources of the Holifield Radioactive Ion Beam Facility, which was a DOE Office of Science User Facility (HRIBF) operated by the Oak Ridge National Laboratory. The authors are grateful to the HRIBF facility operations staff who made the measurements possible.

[1] Connecting Quarks with the Cosmos, The National Academies Press Washington D.C. (2003).

[2] Nuclear Physics: Exploring the Heart of Matter, The National Academies Press, Washington, DC (2013).
[3] A. Arcones *et al.*, Prog. Nucl. Part. Phys. **94**, 1 (2017).
[4] C. J. Horowitz *et al.*, submitted to J. Phys. G (2018).
[5] E. M. Burbidge *et al.*, Rev. Mod. Phys. **29**, 547 (1957).
[6] B. P. Abbott *et al.*, Phys. Rev. Lett. **119**, 161101 (2017).
[7] B. P. Abbott *et al.*, Ap. J. Lett. **848**, L12 (2017).
[8] N. R. Tanvir, Ap. J. Lett. **848**, L27 (2017).
[9] M. Arnould, S. Goriely, and K. Takahashi, Phys. Rep. **450**, 97 (2007).
[10] F. K. Thielemann, Prog. Nucl. Part. Phys. **66**, 346 (2011).
[11] M.R. Mumpower *et al.*, Prog. Nucl. Part. Phys. **86**, 86 (2016).
[12] J. Beun *et al.*, J. Phys. G **36**, 025201 (2009).
[13] R. Surman *et al.*, Phys. Rev. C **79**, 045809 (2009).
[14] R. A. Surman *et al.*, WSPC Proceedings **15**, 5 (2011).
[15] S. Wanajo, et al., Ap. J **852**, 40 (2018).
[16] H. Schatz, J. Phys. G **43**, 064001 (2016).
[17] R. A. Surman, et al., Phys. Rev. Lett. **79**, 10 (1997).
[18] K. L. Jones *et al.*, Nature **465** 454 (2010).
[19] K. L. Jones *et al.*, Phys. Rev. C **84**, 034601 (2011).
[20] R. L. Kozub *et al.*, Phys. Rev. Lett. **109**, 172501 (2012).
[21] J. M. Allmond *et al.*, Phys. Rev. Lett. **112**, 172701 (2014).
[22] G. E. Brown, Nucl. Phys. **57**, 339 (1964).
[23] C. F. Clement, A. M. Lane, and J. R. Rook, Nucl. Phys. **66**, 273 (1965).
[24] W. E. Parker *et al.*, Phys. Rev. C **52**, 252 (1995).
[25] A. Likar and T. Vidmar, Nucl. Phys. A **591**, 458 (1995).
[26] T. Rauscher *et al.*, Phys. Rev. C **57**, 2031 (1998).
[27] I. Tomandl *et al.*, Phys. Rev. C **83**, 044326 (2011).
[28] J. Timar *et al.*, NDS **121**, 143 (2014).
[29] K. Y. Chae *et al.*, Nucl. Instrum. Meth. A **751**, 6 (2014).
[30] D. W. Bardayan *et al.*, Nucl. Instrum. Meth. A **711**, 160 (2013).
[31] B. Manning, PhD dissertation, Rutgers University, (2014).
[32] B. Manning *et al.*, AIP Conference Proceedings **1525**, 548 (2013).
[33] I. J. Thompson, Comp. Phys. Rep. **7**, 167 (1988).
[34] R. V. Reid Jr, Ann. Phys. **50**, 411 (1968).
[35] A. J. Koning and J. P. Delaroche, Nucl. Phys. A **713**, 231 (2003).
[36] R. L. Varner, W. J. Thompson, T. L. McAbee, E. J. Ludwig, and T. B. Clegg, Phys. Rep., **201**, 57, 1991.
[37] M. Igarashi and M. Toyama, Computer program TWOFNR, University of Surrey, modified version (2008).
[38] J. Terasaki *et al.*, Phys. Rev. C **71**, 034310 (2005).
[39] J. S. Thomas *et al.*, Phys. Rev. C **76**, 044302 (2007).
[40] K. L. Jones *et al.*, Phys. Rev. C **70**, 067602 (2004).
[41] S. Ahn *et al.*, submitted for publication, (2017).
[42] G. Arbanas, F. S. Dietrich, A. K. Kerman *Direct-Semidirect Thermal Neutron Capture Calculations*, Perspectives on Nuclear Data for the Next Decade, (2005).
[43] https://www-nds.iaea.org/RIPL-3/.
[44] S. Chiba *et al.*, Phys. Rev. C **77**, 015809 (2008).
[45] H. Koura and M. Yamada, Nucl. Phys. A **671**, 96 (2000).
[46] S. D. Pain *et al.*, Physics Procedia **90**, 455 (2017).
[47] A. Ratkiewicz *et al.*, submitted to Phys. Rev. Lett. (2018).